ELSEVIER

Journal of Hazardous Materials B134 (2006) 257–267

Journal of Hazardous Materials

www.elsevier.com/locate/jhazmat

Characterization of mesoporous rice husk ash (RHA) and adsorption kinetics of metal ions from aqueous solution onto RHA

Vimal Chandra Srivastava, Indra Deo Mall *, Indra Mani Mishra

Department of Chemical Engineering, Indian Institute of Technology Roorkee, Roorkee 247 667, India

Received 18 August 2005; received in revised form 6 November 2005; accepted 8 November 2005
Available online 28 December 2005

Abstract

The present study deals with the characterization of low-cost rice husk ash (RHA) for its various physico-chemical properties and adsorption characteristics of metal ions. The average particle size of RHA was 150.47 μm. Proximate analysis showed the presence of high amount of ash in RHA. Bulk density and the heating value of RHA were 104.9 kg/m^3 and 9.68 MJ/kg, respectively. The pore size distribution results showed that the RHA was predominantly mesoporous. The BET surface area was 36.44 m^2/g. The average pore diameter by BET was 42.603 Å. The BJH pore area showed 80% of the pore area due to the mesopores. The polar groups present on the RHA surface imparted considerable cation exchange capacity to it. RHA was found to be an effective adsorbent for the removal of cadmium (Cd(II)), nickel (Ni(II)) and zinc (Zn(II)) metal ions from aqueous solutions. The pH_0 ≈6.0 is found to be the optimum for the removal of individual cations from the aqueous solutions by RHA at an optimum dose of 10 kg/m^3. The kinetics of adsorption showed that the metal ions adsorption on RHA is a gradual process with quasi-equilibrium being attained in 5 h. The pseudo-second-order kinetics represents the equilibrium data well. The effective diffusion coefficient of the cations onto the RHA is of the order of 10^{-13} m^2/s.

Keywords: Adsorption; Rice husk ash (RHA); Mesoporous material; Kinetics; Metal removal; Cadmium(II); Nickel(II); Zinc(II)

1. Introduction

Excessive release of toxic metals into the environment due to industrialization has created a great global concern. Monitoring and subsequent removal of toxic metals from the industrial effluents has, therefore, been made mandatory before their discharge into the environment. Cadmium (Cd(II)), nickel (Ni(II)) and zinc (Zn(II)) ions in aqueous solutions are toxic. During metal winning and refining of metal ores in zinc, lead and copper smelters, cadmium gets reduced in the environment in the form of metal slag and is also present in dissolved form in wastewaters. Cd(II) is a non-essential and a non-biodegradable component which slowly accumulates in the body, usually through food chain. Nickel is also a common environmental pollutant and is toxic (e.g. in concentrations more than 15 mg/l), especially to activated sludge bacteria, and its presence is detrimental to the operation of anaerobic digesters used in wastewater treatment plants [1]. Cd(II) and Ni(II) ions are frequently encountered together in industrial wastewaters. Zn(II) is not so toxic as Cd(II) or Ni(II), and is considered dangerous probably due to the associated toxic Cd(II) as an impurity [2]. Due to toxicity of these metals, the Ministry of Environment and Forests (MOEF), Government of India has set minimal national standards (MINAS) of 0.2, 2.0, 5.0 mg/l, respectively, for Cd(II), Ni(II) and Zn(II) for safe discharge of the effluents containing these metal ions into surface waters [3].

Various methods used for the removal of metals from wastewaters include chemical precipitation, membrane filtration, ion exchange and adsorption. Adsorption using activated carbon (AC) as an adsorbent has now been regarded as a major process for wastewater treatment. However, due to high cost and about 10–15% loss during AC regeneration, non-conventional and cheap adsorbents like bagasse fly ash (BFA), rice husk ash (RHA), peat, lignite, bagasse pith, wood, saw dust, etc. have been used as alternative adsorbents [4–9].

Rice husk is an agricultural waste, obtained from the rice mills. It accounts for about one-fifth of the annual gross rice

* Corresponding author. Tel.: +91 1332 285319 (O)/285106 (R); fax: +91 1332 276535/273560.
E-mail address: id_mall2000@yahoo.co.in (I.D. Mall).

0304-3894/$ – see front matter © 2005 Published by Elsevier B.V.
doi:10.1016/j.jhazmat.2005.11.052

production of 545 million metric tons, of the world [10]. Rice husk is mostly used as a fuel in the boiler furnaces of various industries to produce steam. The rice husk ash (RHA) is collected from the particulate collection equipment attached upstream to the stack of the rice husk-fired boilers. Since RHA is available in plenty and it has very high potential as an adsorbent, the present study has been undertaken to report in detail the mesoporous characteristics of RHA and its adsorption characteristics for Cd(II), Ni(II) and Zn(II) ions from aqueous solutions. The study also reports the effect of such factors as the initial pH (pH_0), adsorbent dose (m), initial metal ion concentration (C_0), and contact time (t) on the adsorption efficiency of these metal ions from aqueous solutions. The kinetics of adsorption of Cd(II), Ni(II) and Zn(II) on RHA has also been studied and various kinetic models, viz. pseudo-first-order, pseudo-second-order, and intra-particle diffusion models have been for their usefulness in correlating the experimental data.

2. Experimental

2.1. Adsorbent and its characterization

RHA was used as obtained from a nearby paper mill without any pretreatment except sieving to remove very fine particles. The physico-chemical characterization of RHA was performed using standard procedures. Proximate analysis was carried out using the standard procedure [11]. Bulk density was determined by using MAC bulk density meter whereas particle size analysis was done using standard sieves. Carbon, hydrogen and nitrogen (CHN) analysis of RHA was done using Perkin Elmer CHN elemental analyser. X-ray diffraction (XRD) analysis was carried out using Phillips (Holland) diffraction unit (Model PW 1140/90), using copper as the target with nickel as the filter media, and K radiation maintained at 1.542 Å. Goniometer speed was maintained at 1°/min. Scanning electron microscopic (SEM) analysis of RHA was carried out by using a scanning electron microscope (Model SEM-501 Phillips, Holland).

Textural characteristics were determined by nitrogen adsorption at 77.15 K to determine the specific surface area and the pore diameter of the RHA using an ASAP 2010 Micromeritics instrument and by Brunauer-Emmett-Teller (BET) method [12], using the software of Micromeritics. Nitrogen was used as cold bath (77.15 K). The Barrett-Joyner-Hanlenda (BJH) method [13] was used to calculate the mesopore distribution.

FTIR spectrometer (Thermo nicolet, Model Magna 760) was employed to determine the presence of functional groups in RHA at room temperature. Pellet (pressed-disk) technique was used for this purpose. The spectral range chosen was from 4000 to 400 cm^{-1}.

2.2. Adsorbates

All the chemicals used in the study were of analytical reagent (AR) grade. Nickel chloride hexahydrate ($NiCl_2{\cdot}6H_2O$) was procured from Qualigens Fine Chemicals, Mumbai, India. Cadmium sulphate octahydrate ($3CdSO_4{\cdot}8H_2O$), Zinc sulphate heptahydrate ($ZnSO_4{\cdot}7H_2O$), NaOH, and HCl were obtained from S.D. fine Chemicals, Mumbai, India. Stock solutions of Cd(II), Ni(II) and Zn(II) were made by dissolving exact amount of $3CdSO_4{\cdot}8H_2O$, $NiCl_2{\cdot}6H_2O$ and $ZnSO_4{\cdot}7H_2O$ in distilled water, respectively. The range of concentration of metal components prepared from stock solution varied between 50 and 500 mg/l. These test solutions were prepared by diluting 1 g/l of stock solution of Cd(II), Ni(II) and Zn(II) with double-distilled water.

2.3. Batch adsorption studies

For each experimental run, 100 ml aqueous solution of known concentration of either Cd(II) or Ni(II) and Zn(II), as the case may be, was taken in 250 ml conical flask containing 1 g of RHA. These flasks were agitated at a constant shaking rate of 150 rpm in a temperature controlled orbital shaker (Remi Instruments, Mumbai) maintained at 30 °C. The initial pH (pH_0) of the adsorbate solution was adjusted using 1 N (36.5 g/l) HCI or 1 N (40 g/l) NaOH aqueous solution without any further adjustment during the sorption process. To check whether the equilibrium has been attained, the samples were withdrawn from the flasks at different time intervals, centrifuged using a Research Centrifuge (Remi Instruments, Mumbai) at 5000 rpm for 5 min and then the supernatant liquid was analyzed for residual concentration of metal ions using an atomic adsorption spectrophotometer (GBC Avanta Instrument, Australia).

2.4. Point of zero charge

The point of zero charge of the RHA was determined by the solid addition method [14]. To a series of 100 ml conical flasks 45 ml of KNO_3 solution of known strength was transferred. The pH_0 values of the solution were roughly adjusted from 2 to 12 by adding either 0.1 N HNO_3 or NaOH. The total volume of the solution in each flask was made exactly to 50 ml by adding the KNO_3 solution of the same strength. The pH_0 of the solutions were then accurately noted. One gram of RHA was added to each flask, which were securely capped immediately. The suspensions were then manually shaken and allowed to equilibrate for 48 h with intermittent manual shaking. The pH values of the supernatant liquid were noted. The difference between the initial and final pH (pH_f) values ($\Delta pH = pH_0 - pH_f$) was plotted against the pH_0. The point of intersection of the resulting curve at which ΔpH 0 gave the. The procedure was repeated for different concentrations of KNO_3.

2.5. Effect of initial pH (pH_0)

The effect of pH_0 on the sorption was studied by adjusting the pH_0 in the range of 2–10. In these experiments, the RHA loading was kept at 10 g/l of solution containing 100 mg/l each of Cd(II), Ni(II) and Zn(II) at 30 °C. The contact time (t) was kept as 5 h, since equilibrium was found to have been attained at 5 h contact time.

2.6. Analysis of metal ions

The concentration of Cd(II), Ni(II) and Zn(II) in the sample was determined by a flame atomic absorption spectrophotometer (GBC Avanta, Australia) with the detection limit of 0.009, 0.040 and 0.008 mg/l at the wavelengths of 228.8, 232 and 213.9 nm, for Cd(II), Ni(II) and Zn(II), respectively, by using air–acetylene flame. Before the analysis, the sample was diluted to the concentration in the range of 0.2–1.8, 1.8–8 and 0.4–1.5 mg/l for Cd(II), Ni(II) and Zn(II), respectively, with double distilled water. Metal ion concentrations were determined in reference to the appropriate standard metal ion solutions.

The percentage removal of metal ions and equilibrium adsorption uptake in solid phase, q_e (mg/g), were calculated using the following relationships:

$$\text{Percentage metal ions removal} = \frac{100(C_0 - C_e)}{C_0} \quad (1)$$

$$\text{Amount of adsorbed metal ions per } g \text{ of solid, } q_e = \frac{(C_0 - C_e)V}{w} \quad (2)$$

where, C_0 is the initial metal ion concentration (mg/l), C_e is the equilibrium metal ion concentration (mg/l), V is the volume of the solution (l) and w is the mass of the adsorbent (g).

3. Results and discussion

3.1. Characterization of RHA

The particle sizes of RHA were <63 (48.78%), 63–90 (16.54%), 90–125 (11.7%), 125–150 (12.82%), 150–212 (32.56%), 212–300 (1.86%), 300–425 (5.89%), 425–500 (3.58%), 500–600 (0.22%) and >600 (0.05%) μm. Average particle size of RHA was 150.47 μm. Proximate analysis showed the presence of 0.73% moisture, 5.37% volatile matter, 88.0% ash and 5.90% fixed carbon in RHA. High amount of ash indicates that RHA is basically inorganic in nature. Typical composition of inorganic ash is 96.34% SiO_2, 2.31% K_2O, 0.45% MgO, 0.2% Fe_2O_3, 0.41% Al_2O_3 and 0.41% CaO [4]. CHN analysis showed 7.424% carbon, 0.061% hydrogen, 0.846% nitrogen and rest others. Similar properties of RHA have been reported by Nakbanpote et al. [4]. Due to low carbon content, RHA has low porosity and thereby low surface area. Bulk density and heating value of RHA were found to be 104.9 kg/m^3 and 9.68 MJ/kg, respectively. For structural and morphological characteristics, XRD and SEM analyses were carried out. The d-spacing values provided by the XRD spectra of RHA reflected the presence of Cristobalite (SiO_2), Margaritasite ($(Cs,K,H_3O)_2(UO_2)2V_2O_8\cdot(H_2O)$) and Macedonite ($PbTiO_3$). SEM of RHA (Fig. 1) reveals its surface texture and porosity. It shows very fine particle size to the order of a millimeter or less and that there are pores of varying sizes within the particle.

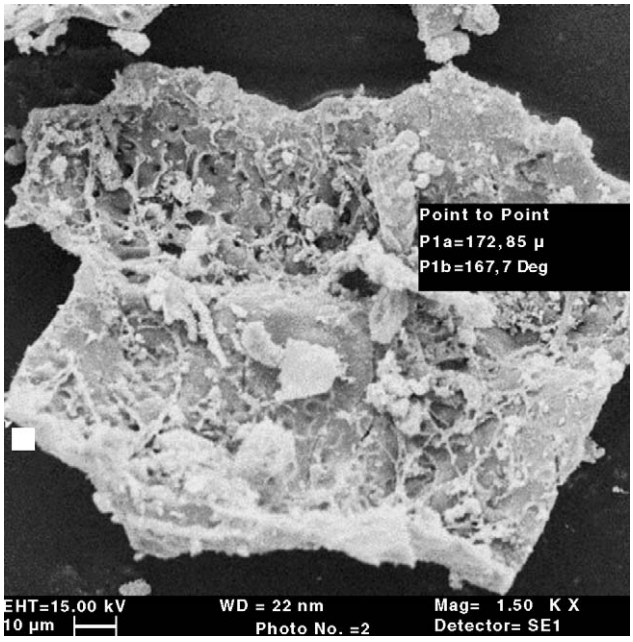

Fig. 1. Scanning electron micrograph of RHA at 1500 X magnification.

3.1.1. Pore size distribution of RHA

BJH method is probably the most popular method used for the evaluation of the mesopore size distribution. Pore sizes are classified in accordance with the classification adopted by the International Union of Pure and Applied Chemistry (IUPAC) [15], that is, micropores (diameter (d) <20 Å), meso-pores (20 Å < d < 500 Å) and macropores (d > 500 Å). Micropores can be divided into ultra-micropores (d < 7 Å) and super-micropores (7 Å < d < 20 Å). Because of the larger sizes of liquid molecules, the adsorbents for liquid phase adsorbates should have predominantly mesopores in the structure [9].

RHA has a wide pore size distribution (Fig. 2) giving wide distribution of surface area. The BET surface area of RHA is 36.44 m^2/g, whereas BJH adsorption/desorption surface area of pores is 27.45/22.18 m^2/g. The single point total pore volume of pores (d < 2178 Å) is found to be 0.0388 cm^3/g, whereas cumulative adsorption/desorption pore volume of the pores (17 Å < d < 3000 Å) is 0.03858/0.03523 cm^3/g, respectively. The analysis of the BJH adsorption pore distribution shows that the

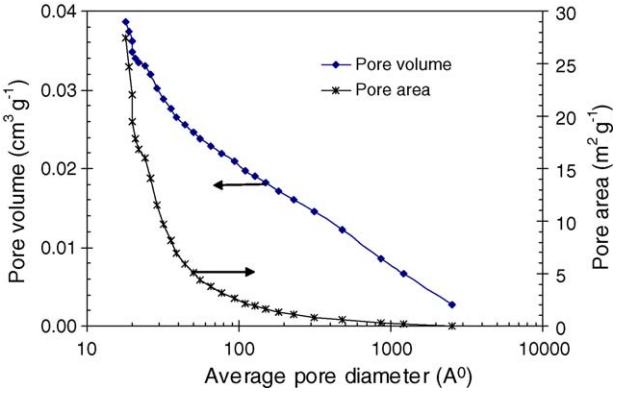

Fig. 2. Pore size distribution of RHA.

micropores ($d < 20$ Å) have a total pore area of about 20%, mesopores account for about 78% and that the macropores about 2%. The desorption pore distribution shows that the mesopores account for 99% of the pore area. The average pore diameter by BET method is found to be 42.603 Å, whereas the BJH adsorption/desorption average pore diameter is 56.222/63.3535 Å. The RHA, thus, is found to consist of mesopores predominantly. This is what is desirable for the liquid phase adsorptive removal of metal ions. The 99% pore area attributed to mesopores during desorption indicates the predominance of mesopores in adsorption process.

3.1.2. FTIR spectroscopy of RHA

The chemical structure of the adsorbent is of vital importance in understanding the adsorption process. The FTIR technique is an important tool to identify the characteristic functional groups, which are instrumental in adsorption of metal ions.

The FTIR spectra of the blank and metal loaded RHA is shown in Fig. 3. This figure shows a broad band between 2800 and 3700 cm^{-1} with little about 3400 and 2920 cm^{-1} which indicate the presence of both free and hydrogen bonded OH groups and Si–OH group on the adsorbent surface. This stretching is due to both the silanol groups (Si–OH) and adsorbed water (peak at 3430 cm^{-1}) on the surface [16]. The stretching of OH groups bound to methyl radicals shows a signal between 2940 and 2820 cm^{-1}. Similarly, peaks around 1470 cm^{-1} are indicative of $–CH_2$ and $–CH_3$ groups while those at 1380 cm^{-1} are indicative of $–CH_3$ groups. The IR spectra indicated weak and broad peaks about 1600 cm^{-1} corresponding to –C=O and –C–OH groups stretching from aldehydes and ketones. The transmittance in the 1050–1300 cm^{-1} region is ascribed to the vibration of the CO group in lactones [17]. The peak at 1300 cm^{-1} band may be attributed to the aromatic CH and carboxyl-carbonate structures [18] and silanol groups. The silanol groups are in the form of silicon dioxide structure (–Si–O–Si–OH). This structure is similar to the silanol groups of silicic acid [4]. The peak at 1100 cm^{-1} is due to Si–O–Si and –C–O–H stretching and –OH deformation. The presence of polar groups on the surface is likely to give considerable cation exchange capacity to the adsorbents [19]. The peaks at about 793 and 469 cm^{-1} indicate the presence of Si–H. With the loading of metal ions the shifting of the peaks is seen from about 3430, 2920, 1636, 1092, 792 and 468 cm^{-1}. This means that the functional groups at these wave numbers participate in the metal adsorption. The shifting occurs both to higher and lower wave numbers. The FTIR spectra for Cd-loaded RHA shows the disappearance of bonds around 2900 and 1636 cm^{-1}, and shifting of bands about 1092, 792 and 468 cm^{-1} to lower wave numbers. Such disappearance of bands is not observed in the Ni- and Zn-loaded RHA spectra, although the shifting of all the bands is visible. These characteristics indicate that –CO–, –OH, –Si–OH, –SiH and –C–OH groups are effective in the adsorption Cd(II), Ni(II) and Zn(II) onto RHA.

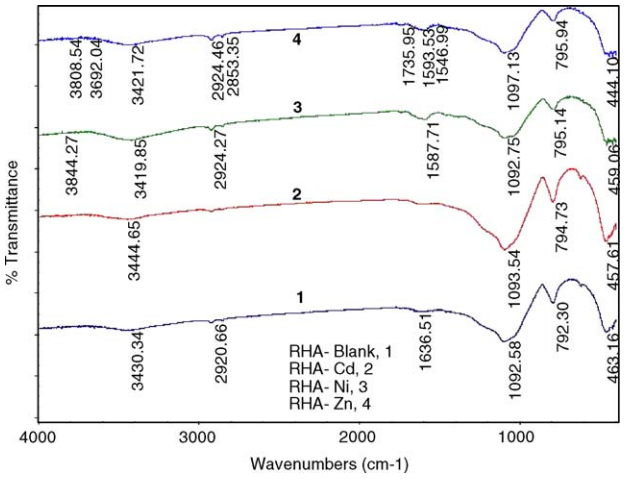

Fig. 3. FTIR spectroscopy of blank and metal ion loaded RHA.

3.2. Effect of initial pH (pH_0)

The pH of the solution affects the surface charge of the adsorbents as well as the degree of ionization and speciation of different pollutants [20]. Change in pH affects the adsorptive process through dissociation of functional groups on the active sites on the surface of the adsorbent. This subsequently leads to a shift in reaction kinetics and the equilibrium characteristics of the adsorption process. Adsorption of various anionic and cationic species on such adsorbents can be explained on the basis of the competitive adsorption of H^+ and OH^- ions with the adsorbates. It is a common observation that the surface adsorbs anions favourably at lower pH due to presence of H^+ ions, whereas, the surface is active for the adsorption of cations at higher pH due to the deposition of OH^- ions.

To understand the adsorption mechanism, it is necessary to determine the point of zero charge (pH_{PZC}) of the adsorbent. Adsorption of cations is favored at $pH > pH_{PZC}$, while the adsorption of anions is favored at $pH < pH_{PZC}$. The specific adsorption of cations shifts towards lower values, whereas the specific adsorption of anions shifts towards higher values. Fig. 4 shows that for all the concentrations of KNO_3, the zero value of ΔpH lies at the initial pH value of 8.3, which is considered as the of the adsorbent.

The influence of the pH_0 of metal ion solution on the extent of adsorption of Cd(II), Ni(II) and Zn(II) ions onto RHA is shown in Fig. 5. Adsorption of metal ions increases with increase in pH_0.

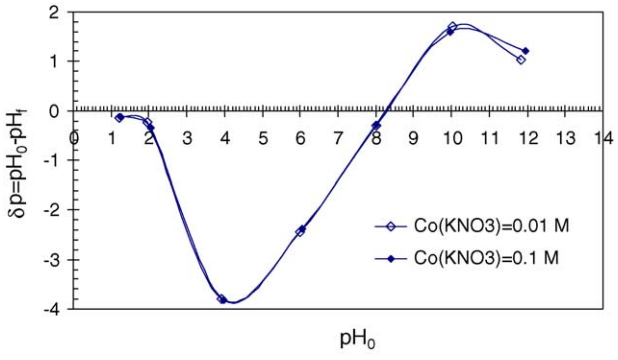

Fig. 4. Point of zero charge of RHA.

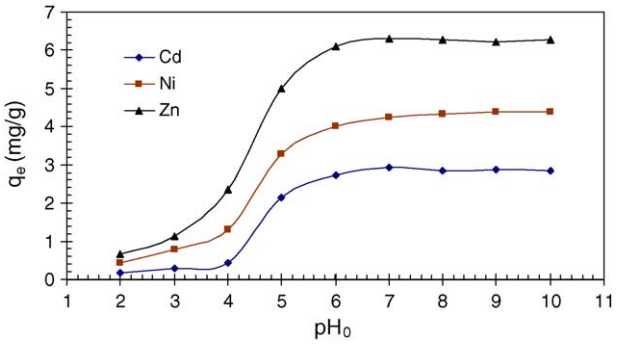

Fig. 5. Effect of pH_0 for the removal of Cd(II), Ni(II) and Zn(II) by RHA (T = 303 K, t = 5 h, C_0 = 100 mg/l, m = 10 g/l).

Up to pH_0 4, the increase in adsorption is gradual, which, however, increases drastically for $pH_0 > 4$. At higher pH_0 ($\geq$6.0), Cd(II), Ni(II) and Zn(II) ion adsorption was nearly constant throughout. The pH of the solution changes during the time-course of metal sorption onto RHA. Fig. 6 shows the variation in pH for the adsorption of Cd(II), Ni(II) and Zn(II) with the contact time upto 10 h. It can be seen that the pH of the solution rises sharply during the initial 30 min of sorption process, and, thereafter, the pH of the solution remains invariant for all the three metal cations.

The adsorption of metal ions on a hydrous oxide surface can be explained on the basis of the surface complex formation model. The hydrolysis of silicon dioxide produces hydrous oxide surface group –SiOH i.e., the silanol group. This results in the formation of a weakly acidic silica surface with pK_a = 6–8 [21]. As silica is one of the important constituent of RHA, the sorption of metal ions can take place by the cation exchange reaction through the substitution of protons from silanol groups on the surface by the metal ions from the solution, as follows

$$m(-\mathrm{SiOH}) \leftrightarrow m(-\mathrm{SiO^-}) + m\mathrm{H^+} \quad (3)$$

$$\mathrm{M}^{n+} + m(-\mathrm{SiO^-}) \leftrightarrow \mathrm{M(OSi-)}_m{}^{(n-m)+} \quad (4)$$

The overall reaction can thus be represented as:

$$\mathrm{M}^{n+} + m(-\mathrm{SiOH}) \leftrightarrow \mathrm{M(OSi-)}_m{}^{(n-m)+} + m\mathrm{H^+} \quad (5)$$

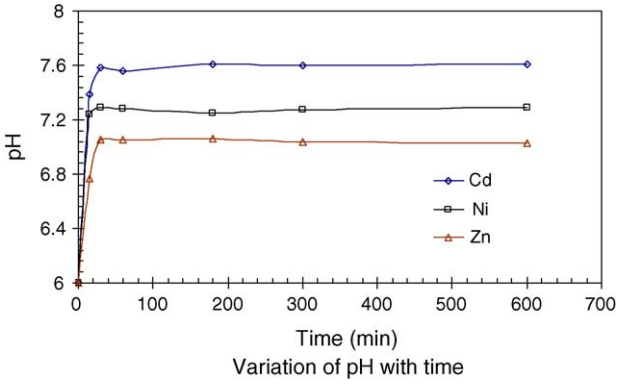

Fig. 6. Variation of pH with time for the removal of Cd(II), Ni(II) and Zn(II) by RHA (pH_0 = 6.0, T = 303 K, t = 5 h, C_0 = 100 mg/l, m = 10 g/l).

where M^{n+} = metal ion with n^+ charge, –SiOH = silanol group on SiO_2 surface, $m\mathrm{H^+}$ = number of protons released. Although the ion-exchange reaction is able to explain the sorption process, metal sorption on the RHA may also take place through complex formation on the cell surface after interaction between the metal and active groups present on RHA surface [22].

It can be observed from Fig. 6 that the pH of the solution always increases during sorption process because of simultaneous and, perhaps competitive adsorption of metal cations and H^+ ions onto RHA. The sorption profile of metal ions on RHA as a function of the pH_0 (Fig. 5) could also be explained on the basis of surface charge density of silanol groups and other functional groups, such as hydroxyl, carboxyl, amino and others. As observed in Fig. 3, it seems that all these groups are participating in the adsorption as the peaks of the band corresponding to these groups shift when RHA gets loaded with the metal ions as explained earlier. The increase in adsorption with the increase in pH_0 can be attributed to the fact that the positively charged metal cations are repulsed less by the oxide surfaces at higher pH values. The removal of metal ions could, therefore, be the net result of the "ion exchange" and "surface complexation" phenomena occurring on the surface of the RHA. Similar results have been observed for the adsorption of lead on rice husks [23]. The removal of the cations was in the order: Zn(II) > Ni(II) > Cd(II) (Fig. 5). The trend is according to decreasing size of the metal ions: Cd(II) (1.71 Å) < Ni(II) (1.62 Å) < Zn(II) (1.53 Å). Smaller size metal ions could get adsorbed more deeply into pores big enough not to adsorb much greater size metal ions. Since RHA is predominantly mesoporous, most of the cations get adsorbed into mesopores.

3.3. Effect of adsorbent dosage (m)

The effect of m on the uptake of Cd(II), Ni(II) and Zn(II) ions onto RHA was studied and is shown in Fig. 7. This figure reveals that the removal of metal ions increases with increase in adsorbent dosage from 1 to 10 g/l. The removal remains unchanged above 10 g/l of RHA dosage. An increase in the adsorption with the adsorbent dosage can be attributed to the availability of greater surface area and more adsorption sites. At m < 7 g/l, the adsorbent surface becomes saturated with metal ions and the residual metal ion concentration in the solution is large.

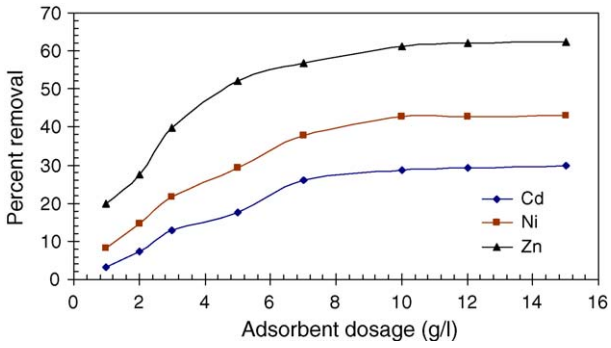

Fig. 7. Effect of adsorbent dose on the removal of Cd(II), Ni(II) and Zn(II) by RHA (T = 303 K, t = 5 h, C_0 = 100 mg/l).

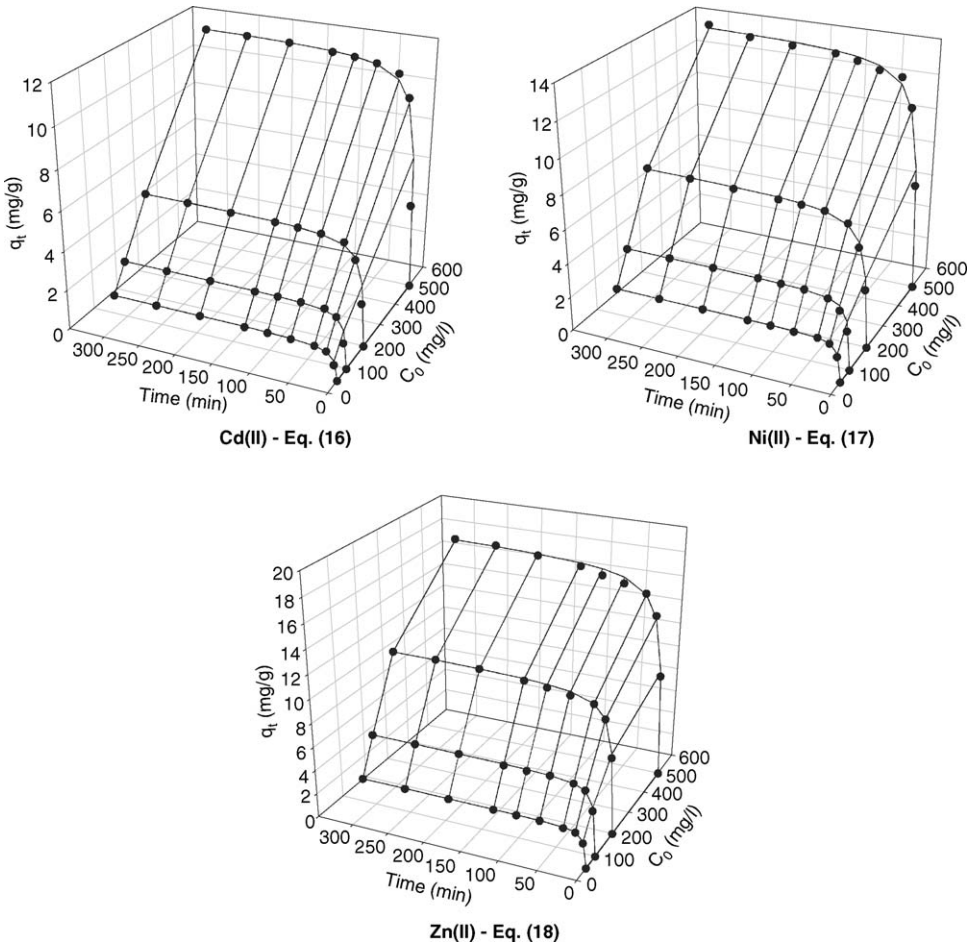

Fig. 8. Comparison of experimental data points given by symbols and the surface predicted by the model given by Eqs. (16)–(18).

With an increase in m, the metal ions removal increases due to increased metal ions uptake by the increased amount of adsorbent. At $m > 7$ g/l, the incremental metal ions removal becomes very low, as the surface metal ions concentration and the solution metal ion concentration come to equilibrium with each other. At about $m = 10$ g/l, the removal efficiency becomes almost constant. Maximum removal of metal cations at $C_0 = 100$ mg/l was found to be 62.5% for Zn(II), 43.1% for Ni(II) and 29.8% for Cd(II).

3.4. Effect of initial metal ion concentration (C_0)

The effect of C_0 on the extent of adsorption of Zn(II) onto RHA as a function of time is shown in Fig. 8. At any time the amount of Zn(II) ions adsorbed per unit mass of adsorbent increases with increasing C_0. The C_0 provides the necessary driving force to overcome the resistances to the mass transfer of Zn(II) ions between the aqueous and the solid phases. The increase in C_0 also enhances the interaction between Zn(II) ion and the RHA. Therefore, an increase in C_0 of Zn(II) enhances the adsorption uptake of Zn(II). Similar trends have been observed for Cd(II) and Ni(II) adsorption onto RHA also. The maximum cation removal at $C_0 = 500$ mg/l is found to be 35.3% for Zn(II), 27.8% for Ni(II) and 23.3% for Cd(II).

3.5. Effect of contact time

Aqueous metal ion solutions with different C_0 were kept in contact with the adsorbents for 24 h. The residual concentrations at 5 h contact time were found to be higher by a maximum of ∼1% than those obtained after 24 h contact time. Therefore, after 5 h contact time, a steady state approximation was assumed and a quasi-equilibrium situation was accepted. Accordingly all the batch experiments were conducted with a contact time of 5 h under vigorous shaking conditions. Fig. 8 presents the time-course of cations with varying initial concentrations, C_0. The rate of cation removal is found to be very rapid during the initial 15 min, and thereafter, the rate of metal ions removal decreases. No significant change in metal ion removal is observed after about 120 min. It is also found that the adsorptive removal of the metal ions ceases after 300 min of contacting with the RHA. During the initial stage of sorption, a large number of vacant surface sites are available for adsorption. After lapse of some time, the remaining vacant surface sites are difficult to be occupied due to repulsive forces between the solute molecules on the solid surface and the bulk phase. Besides, the metal ions are adsorbed into the mesopores that get almost saturated with metal ions during the initial stage of adsorption. Thereafter, the metal ions have to traverse farther and deeper into the pores encoun-

tering much larger resistance. This results in the slowing down of the adsorption during the later period of adsorption.

3.6. Kinetics of adsorption kinetic study

The frequently used kinetic models, viz. pseudo-first-order, pseudo-second-order and intraparticle diffusion models, have been tested to investigate the adsorption process of Cd(II), Ni(II) and Zn(II) on RHA.

3.6.1. Pseudo-first-order model

The sorption of molecules from a liquid phase to a solid phase can be considered as a reversible process with equilibrium being established between the solution and the solid phase. Assuming a non-dissociating molecular adsorption of metal ions on RHA particles, the sorption phenomenon can be described as the diffusion controlled process.

$$A + S \underset{k_D}{\overset{k_A}{\rightleftharpoons}} AS \tag{6}$$

where, A is the adsorbate and S is the active site on the adsorbent and AS is the activated complex. k_A and k_D are the adsorption and desorption rate constants, respectively. Using first order kinetics it can be shown that with no adsorbate initially present on the adsorbent (i.e., $C_{AS0} = 0$ at $t = 0$), the fractional uptake of the adsorbate by the adsorbent can be expressed as

$$\frac{X_A}{X_{Ae}} = 1 - \exp\left(k_A C_S + \frac{k_A}{K_S}\right) t \tag{7}$$

where X_{Ae} is the fraction of the adsorbate adsorbed on the adsorbent under equilibrium condition,

$K_S = k_A/k_D$; C_S is the adsorbent concentration in the solution

Eq. (7) can be transformed as

$$\log(q_e - q_t) = \log q_e - \frac{k_f}{2.303} t \tag{8}$$

where

$$k_f = \left(k_A C_S + \frac{k_A}{K_S}\right); \tag{9}$$

$q = X_A$, and $q_e = X_{Ae}$

The values of the first-order adsorption rate constant (k_f) (Tables 1–3) were determined from Eq. (8) by plotting $\log(q_e - q_t)$ against t (not shown) for Cd(II), Ni(II) and Zn(II) ions adsorption on RHA with $C_{A0} = 50$, 100, 200 and 500 mg/l at 30 °C.

3.6.2. Pseudo-second-order model

The pseudo-second-order model can be represented in the following form [24]:

$$\frac{dq_t}{dt} = k_S(q_e - q_t)^2 \tag{10}$$

where, k_S is the pseudo-second-order rate constant (g/mg min). The integration of Eq. (10) with the boundary conditions, $q_t = 0$ at $t = 0$ and $q_t = q_t$ at $t = t$, results in the following equation:

$$\frac{t}{q_t} = \frac{1}{k_S q_e^2} + \frac{1}{q_e} t \tag{11}$$

The initial sorption rate, h (mg/g min), at $t \to 0$ can be defined as

$$h = k_S q_e^2 \tag{12}$$

Eq. (11) can be rearranged to get:

$$q_t = \frac{t}{1/h + (1/q_e)t} \tag{13}$$

q_e is obtained from the slope of the t/q_t versus t plot (Fig. 9), and h is obtained from the intercept. Since q_e is known from the slope, k_S can be determined from the value of h. The best-fit values of h, q_e and k_S along with the correlation coefficients for the pseudo-first-order and pseudo-second-order models are shown in Tables 1–3. The $q_{e,exp}$ and the $q_{e,cal}$ values for the pseudo-first-order model and pseudo-second-order models are also shown in Tables 1–3. The $q_{e,exp}$ and the $q_{e,cal}$ values from the pseudo-second-order kinetic model are very close to each other. The calculated correlation coefficients are also closer to unity for pseudo-second-order kinetics than that for the pseudo first-order kinetic model. Therefore, the sorption can be approximated more appropriately by the pseudo-second-order kinetic model than the first-order kinetic model for the adsorption of Cd(II), Ni(II) and

Table 1
Kinetic parameters for the removal of Cd(II) by RHA ($T = 303$ K, $C_0 = 50$, 100, 200 and 500 mg/l, $m = 10$ g/l)

Pseudo-first-order model

C_0 (mg/l)	$q_{e,exp}$ (mg/g)	$q_{e,calc}$ (mg/g)	k_f (min^{-1})	R_2^2 (non-linear)
50	1.665	0.4758	0.0199	−0.9752
100	2.930	0.4989	0.0178	−0.9165
200	5.480	1.2042	0.0154	−0.9105
500	11.650	2.4912	0.0178	−0.9350

Pseudo-second-order model

C_0 (mg/l)	$q_{e,calc}$ (mg/g)	h (mg/g min)	k_S (g/mg min)	R_2^2 (non-linear)
50	1.6844	0.4288	0.1511	0.9999
100	2.9552	1.0470	0.1198	0.9998
200	5.5347	1.3928	0.0454	0.9998
500	11.7862	3.1789	0.0228	0.9998

Intra-particle diffusion model

C_0 (mg/l)	$k_{id,1}$ (mg/g min$^{1/2}$)	I_1 (mg/g)	R_2^2 (non-linear)
50	0.0501	1.1861	0.9559
100	0.0864	2.2175	0.9080
200	0.2325	3.5153	0.9135
500	0.3598	8.4997	0.9253

C_0 (mg/l)	$k_{id,2}$ (mg/g min$^{1/2}$)	I_2 (mg/g)	R_2^2 (non-linear)
50	0.0101	1.5010	0.9336
100	0.0095	2.7716	0.9747
200	0.0227	5.0853	0.9966
500	0.0445	10.907	0.9775

Table 2
Kinetic parameters for the removal of Ni(II) by RHA (T = 303 K, C_0 = 50, 100, 200 and 500 mg/l, m = 10 g/l)

Pseudo-first-order model

C_0 (mg/l)	$q_{e,exp}$ (mg/g)	$q_{e,calc}$ (mg/g)	k_f (min^{-1})	R_2^2 (non-linear)
50	2.420	0.4079	0.0177	−0.9409
100	4.235	0.9173	0.0232	−0.9664
200	7.968	2.0227	0.0123	−0.9017
500	13.900	3.1602	0.0101	−0.8708

Pseudo-second-order model

C_0(mg/l)	$q_{e,calc}$ (mg/g)	h (mg/g min)	k_S (g/mg min)	R_2^2 (non-linear)
50	2.4311	1.1309	0.1913	0.9999
100	4.2762	1.6039	0.0877	0.9999
200	8.0165	1.6425	0.0256	0.9998
500	13.8947	3.0213	0.0156	0.9997

Intra-particle diffusion model

C_0(mg/l)	$k_{id,1}$ (mg/g min$^{1/2}$)	I_1 (mg/g)	R_2^2 (non-linear)
50	0.0550	1.9284	0.8674
100	0.1921	2.7055	0.9423
200	0.4184	4.3421	0.9379
500	0.4518	9.3919	0.8660

C_0(mg/l)	$k_{id,2}$ (mg/g min$^{1/2}$)	I_2 (mg/g)	R_2^2 (non-linear)
50	0.0082	2.2816	0.9895
100	0.0103	4.0678	0.9320
200	0.0532	7.0201	0.9927
500	0.0999	12.0670	0.9598

Table 3
Kinetic parameters for the removal of Zn(II) by RHA (T = 303 K, C_0 = 50, 100, 200 and 500 mg/l, m = 10 g/l)

Pseudo-first-order model

C_0(mg/l)	$q_{e,exp}$ (mg/g)	$q_{e,calc}$ (mg/g)	k_f (min^{-1})	R_2^2 (non-linear)
50	3.170	0.4494	0.0158	−0.9332
100	6.130	1.2407	0.0193	−0.9624
200	11.700	3.6148	0.0209	−0.9849
500	17.650	6.0583	0.0183	−0.9700

Pseudo-second-order model

C_0(mg/l)	$q_{e,calc}$ (mg/g)	h (mg/g min)	k_S (g/mg min)	R_2^2 (non-linear)
50	3.1819	1.6503	0.1630	1
100	6.1672	2.4329	0.0640	0.9999
200	11.8220	3.1193	0.0223	0.9999
500	17.8440	3.6616	0.0115	0.9998

Intra-particle diffusion model

C_0(mg/l)	$k_{id,1}$ (mg/g min$^{1/2}$)	I_1 (mg/g)	R_2^2 (non-linear)
50	0.0713	2.5320	0.9902
100	0.1487	4.8028	0.9703
200	0.3474	8.2801	0.9259
500	0.5585	11.884	0.9265

C_0(mg/l)	$k_{id,2}$ (mg/g min$^{1/2}$)	I_2 (mg/g)	R_2^2 (non-linear)
50	0.0093	3.0125	0.9664
100	0.0323	5.6030	0.9599
200	0.0771	10.4524	0.9450
500	0.1573	15.0624	0.9664

Zn(II) ions onto RHA. Experimental results did not follow first-order kinetics given by Eq. (8) as there was difference in two important aspects: (i) $k_f(q_e - q_t)$ does not represent the number of available sites, and (ii) log q_e was not equal to the intercept of the plot of $\log(q_e - q_t)$ against t. Mathialagan and Viraraghavan [25] and Taty-Costodes et al. [26] have reported k_S values of 0.061 and 0.3052 g/mg min for Cd(II) adsorption on perlite and sawdust of *Pinus sylerstris*, respectively. k_S values in the range of 0.0083–0.0215 g/mg min have been reported by Padmavathy et al. [27] for the adsorption of Ni(II) onto baker's yeast. But due to different C_e in the nature of the adsorbate-adsorbent systems, a direct comparison of k_S between values obtained in this study with those reported in literature is not possible.

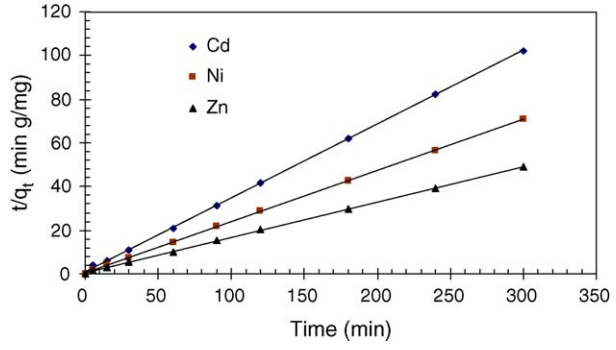

Fig. 9. Pseudo second-order kinetic plot for the removal of Cd(II), Ni(II) and Zn(II) by RHA (T = 303 K, C_0 = 100 mg/l, m = 10 g/l).

Linear plots of q_e and h against C_0 were regressed to obtain these values in terms of initial Cd(II) metal concentration with high coefficient of regression (>0.9969). Therefore, for Cd(II), q_e and h can be expressed as a function of C_0 as follows:

$$q_{e,Cd} = 0.06C_{0,Cd}^{0.85} \quad (14)$$

$$h_{Cd} = -1 \times 10^{-6}C_{0,Cd}^2 + 0.0066C_{0,Cd} + 0.2151 \quad (15)$$

Substituting the value of $q_{e,Cd}$ and h_{Cd} into Eq. (13), the relationship of $q_{t,Cd}$, $C_{0,Cd}$ and t can be represented as follows:

$$q_{t,Cd} = \frac{t}{1/(-1 \times 10^{-6}C_{0,Cd}^2 + 0.0066C_{0,Cd} + 0.2151) + 16.67C_{0,Cd}^{0.85}t} \quad (16)$$

This equation can be used to derive the sorption capacity, q_t at any given $C_{0,Cd}$ and t. Similar equations derived for Ni(II) and Zn(II) ion adsorption onto RHA are as follows:

$$q_{t,Ni} = \frac{t}{1/(-4 \times 10^{-5}C_{0,Ni}^2 + 0.0471C_{0,Ni} + 0.091) + (1/(2 \times 10^{-6}C_{0,Ni}^2 + 0.0026C_{0,Ni} + 1.1146))t} \quad (17)$$

$$q_{t,\mathrm{Zn}} = \frac{t}{1/(-8\times10^{-5}C_{0,\mathrm{Zn}}^2 + 0.0786C_{0,\mathrm{Zn}} - 0.0584) + (1/(-2\times10^{-5}C_{0,\mathrm{Zn}}^2 + 0.0141C_{0,\mathrm{Zn}} + 1.0659))t} \quad (18)$$

Fig. 8 presents the comparison of experimental data with the metal predictions for all the metal ions sorption. A very good fit is found between the data and the predictions.

3.7. Intra-particle diffusion study

The adsorbate transport from the solution phase to the surface of the adsorbent particles occurs in several steps. The overall adsorption process may be controlled either by one or more steps, e.g. film or external diffusion, pore diffusion, surface diffusion and adsorption on the pore surface, or a combination of more than one step. In a rapidly stirred batch adsorption, the diffusive mass transfer can be related by an apparent diffusion coefficient, which will fit the experimental sorption-rate data. Generally, a process is diffusion controlled if its rate is dependent upon the rate at which components diffuse towards one another. The possibility of intra-particle diffusion was explored by using the intra-particle diffusion model [28].

$$q_t = k_{\mathrm{id}}t^{0.5} + I \quad (19)$$

where k_{id} is the intra-particle diffusion rate constant (mg/g min$^{0.5}$) and I (mg/g) is a constant that gives idea about the thickness of the boundary layer, i.e., larger the value of I the greater is the boundary layer effect [29]. If the Weber-Morris [28] plot of q_t versus $t^{0.5}$ satisfies the linear relationship with the experimental data, then the sorption process is found be controlled by intra-particle diffusion only. However, if the data exhibit multi-linear plots, then two or more steps influence the sorption process. The mathematical dependence of fractional uptake of adsorbate on $t^{0.5}$ is obtained if the sorption process is considered to be influenced by diffusion in the cylindrical (or spherical) and convective diffusion in the adsorbate solution. It is assumed that the external resistance to mass transfer surrounding the particles is significant only in the early stages of adsorption. This is represented by first sharper portion. The second linear portion is the gradual adsorption stage with intra-particle diffusion dominating.

Fig. 10 presents the plots of q_t versus $t^{0.5}$ for all the adsorbates. In the figure the data points are related by two straight lines—the first straight portion depicting macropore diffusion and the second representing meso-pore diffusion. These show only the pore diffusion data. Extrapolation of the linear portions of the plots back to the y-axis gives the intercepts which provide the measure of the boundary layer thickness. The deviation of straight lines from the origin (Fig. 10) may be due to difference in rate of mass transfer in the initial and final stages of adsorption. Further, such deviation of straight line from the origin indicates that the pore diffusion is not the sole rate-controlling step. The adsorption data for q versus $t^{1/2}$ for the initial period show curvature, usually attributed to boundary layer diffusion effects or external mass transfer effects [30–31]. The slope of

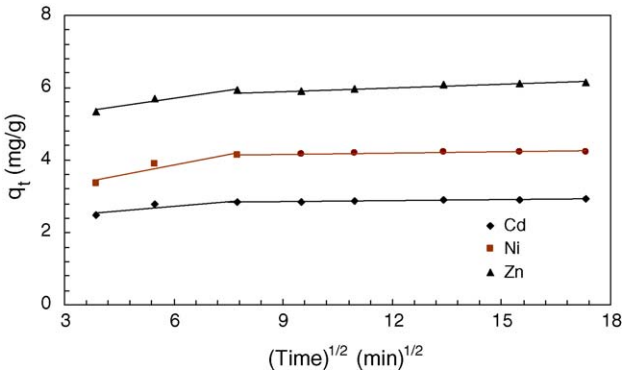

Fig. 10. Weber and Morris intra-particle diffusion plot for the removal of Cd(II), Ni(II) and Zn(II) by RHA (T = 303 K, C_0 = 100 mg/l, m = 10 g/l).

the Weber and Morris plots—q_t versus $t^{0.5}$—are defined as a rate parameter, characteristic of the rate of adsorption in the region where intra-particle diffusion is rate controlling. The values of rate parameters ($k_{\mathrm{id},1}$ and $k_{\mathrm{id},2}$) as given in Tables 1–3 show that $k_{\mathrm{id},1}$ and $k_{\mathrm{id},2}$ values are, generally, higher for lower C_0. The values of the correlation coefficients are also given in Tables 1–3. They show that the Weber-Morris model shows better representation of the data than the pseudo-first order kinetic model.

3.7.1. Determination of diffusivity

Kinetic data could be treated by models given by Boyd et al. [32], which is valid under the experimental conditions used. With diffusion found to be rate controlling in the adsorption of metal ions onto the particles of spherical shape, the solution of the simultaneous set of differential and algebric equations leads to

$$F(t) = 1 - \frac{6}{\pi^2}\sum_{z=1}^{\infty}\frac{1}{z^2}\exp\left(\frac{-z^2\pi^2 D_{\mathrm{e}}t}{R_{\mathrm{a}}^2}\right) \quad (20)$$

where $F(t) = q_t/q_{\mathrm{e}}$ is the fractional attainment of equilibrium at time t, D_{e} is the effective diffusion coefficient of adsorbates in the adsorbent phase (m^2/s), R_{a} is radius of the adsorbent particle assumed to be spherical (m), and z is an integer. The RHA particles are not spherical; they may be taken as cylindrical particles. If one assumes that the diffusion takes place radially with diffusion in the angular and axial direction to be negligible, one gets the solution given by Skelland [33], which after rearrangement is

$$F(t) = 1 - \frac{4}{\pi^2}\sum_{z=1}^{\infty}\frac{1}{b_n^2}\exp(-D_{\mathrm{e}}b_n^2 t) \quad (21)$$

where b_n's are roots of $J_0(bn_pR = 0)$

Vermeulen's approximation [34] of the Eq. (20) fits the whole range $0 < F(t) < 1$, for adsorption on spherical particles.

$$F(t) = \left[1 - \exp\left(\frac{-\pi^2 D_{\mathrm{e}}t}{R_{\mathrm{a}}^2}\right)\right]^{1/2} \quad (22)$$

Table 4
Comparison of effective pore diffusivity for the adsorption of metal ions onto various adsorbents

Adsorbent	Adsorbate	Conditions	$D_e \times 10^{10}$ (m^2/s)	Reference
Solanum nigrum	Cu(II)	$T = 25\,^{\circ}C$, pH 5.5	0.02	[35]
Granular AC[a]	Cu(II)	pH 6, $T = 25\,^{\circ}C$	0.05	[36]
Granular AC[a]	Zn(II)	pH 4.5, $T = 25\,^{\circ}C$	0.5	[36]
Granular AC[a]	Co(II)	pH 3, $T = 25\,^{\circ}C$	3	[36]
Peat	Co(II)	pH 4.5, $T = 25\,^{\circ}C$	1.8	[37]
Peat	Ni(II)	pH 4.5, $T = 25\,^{\circ}C$	2.8	[37]
Peat	Pb(II)	pH 4.5, $T = 25\,^{\circ}C$	4.4	[37]
Bone Char	Cd(II)	pH 4.9, $T = 20\,^{\circ}C$	1.22	[38]
Bone Char	Cu(II)	pH 4.9, $T = 20\,^{\circ}C$	1.41	[38]
Bone Char	Zn(II)	pH 4.9, $T = 20\,^{\circ}C$	1.28	[38]
RHA		pH 6, $T = 30\,^{\circ}C$		Present work
RHA	Cd(II)	$C_0 = 50$ mg/l	7.3361×10^{-3}	Present work
RHA	Cd(II)	$C_0 = 100$ mg/l	6.5285×10^{-3}	Present work
RHA	Cd(II)	$C_0 = 200$ mg/l	5.5644×10^{-3}	Present work
RHA	Cd(II)	$C_0 = 500$ mg/l	6.5011×10^{-3}	Present work
RHA	Ni(II)	$C_0 = 50$ mg/l	6.5546×10^{-3}	Present work
RHA	Ni(II)	$C_0 = 100$ mg/l	8.6109×10^{-3}	Present work
RHA	Ni(II)	$C_0 = 200$ mg/l	4.3768×10^{-3}	Present work
RHA	Ni(II)	$C_0 = 500$ mg/l	3.5790×10^{-3}	Present work
RHA	Zn(II)	$C_0 = 50$ mg/l	5.8357×10^{-3}	Present work
RHA	Zn(II)	$C_0 = 100$ mg/l	7.1494×10^{-3}	Present work
RHA	Zn(II)	$C_0 = 200$ mg/l	7.7148×10^{-3}	Present work
RHA	Zn(II)	$C_0 = 500$ mg/l	6.6917×10^{-3}	Present work

[a] AC (activated carbon).

This equation could further be simplified to cover most of the data points for calculating effective particle diffusivity.

$$\ln\left[\frac{1}{(1 - F^2(t))}\right] = \frac{\pi^2 D_e t}{R_a^2} \tag{23}$$

Thus, the slope of the plot of $\ln[1/(1–F^2(t))]$ versus t would give D_e. Table 4 also presents the values of effective diffusion coefficient (D_e) as calculated from Eq. (23). Average value of D_e are found to be 6.482, 5.780 and 6.848×10^{-13} m^2/s, respectively, for the adsorption of Cd(II), Ni(II) and Zn(II) ions onto RHA. This shows that Zn(II) ions have highest overall pore diffusion rate. Table 4 also gives a comparison of the D_e values as reported by different investigators for different metal cations-adsorbent systems at different experimental conditions of temperature and pH. It may be seen that the pore diffusivities of Cd(II), Ni(II) and Zn(II) for RHA are about two to three order of magnitude lower than those reported in the literature.

4. Conclusion

The present study shows that the RHA is a predominantly mesoporous material accounting for about 80% pore area to mesoporous pores. The –OH, –C–OH and Si–O–Si and Si–H groups present on the RHA surface imparted considerable metal cation exchange capacity to it. The most critical parameter for the process of heavy metal uptake by adsorbents is the pH_0 of the adsorbate solution. Maximum sorption for all the cations, viz. Cd(II), Ni(II) and Zn(II) was found to occur at pH_0 6.0. Equilibrium between the metal ions in the solution and on the RHA surface was practically achieved in 5 h. Maximum metal ions removal at $C_0 = 500$ mg/l at 10 kg/m^3 adsorbent dosage is found to be 35.3% for Zn(II), 27.8% for Ni(II) and 23.3% for Cd(II). Adsorption kinetics followed a second-order rate expression. The adsorption processes could well be described by a two-stage diffusion model. It may be concluded that RHA can be used for the individual removal of Cd(II), Ni(II) and Zn(II) ions from metal-containing effluents.

Acknowledgements

Authors are thankful to the Ministry of Human Resource and Development, Government of India, for providing financial support to undertake this research work.

References

[1] J.W. Patterson, Wastewater Treatment, Science Publishers, New York, 1977.
[2] S.P. Mishra, D. Tiwari, R.S. Dubey, The uptake behaviour of rice (jaya) husk in the removal of Zn(II) ions a radiotracer study, Appl. Radiat. lsot. 48 (7) (1997) 877–882.
[3] MINAS, Pollution control acts, rules, notification issued there under central pollution control Board, Ministry of Environment and Forests, Govt. of India, New Delhi. Sep. 2001.
[4] W. Nakbanpote, P. Thiraveetyan, C. Kalambaheti, Preconcentration of gold by rice husk ash, Miner. Eng. 13 (4) (2000) 391–400.
[5] I.D. Mall, V.C. Srivastava, N.K. Agarwal, I.M. Mishra, Adsorptive removal of malachite green dye from aqueous solution by bagasse fly ash and activated carbon—kinetic study and equilibrium isotherm analyses, Colloid Surf. A: Physicochem. Eng. Aspects 264 (2005) 17–28.
[6] I.D. Mall, V.C. Srivastava, N.K. Agarwal, I.M. Mishra, Removal of congo red from aqueous solution by bagasse fly ash and activated carbon: kinetic study and equilibrium isotherm analyses, Chemosphere 61 (2005) 492–502.
[7] I.D. Mall, V.C. Srivastava, N.K. Agarwal, Removal of orange-G and methyl violet dyes by adsorption onto bagasse fly ash- kinetic study

and equilibrium isotherm analyses, Dyes Pigments 69 (2006) 210–223.
[8] V.C. Srivastava, I.D. Mall, I.M. Mishra, Treatment of pulp and paper mill wastewaters with poly aluminium chloride and bagasse fly ash, Colloid Surf. A: Physicochem. Eng. Aspects 260 (2005) 17–28.
[9] V.C. Srivastava, B. Prasad, I.D. Mall, M. Mahadevswamy, I.M. Mishra, Adsorptive removal of phenol by bagasse fly ash and activated carbon: equilibrium, kinetics and thermodynamics, Colloid Surface A: Physicochem. Eng. Aspects 272 (2006) 89–104.
[10] Q. Feng, Q. Lin, F. Gong, S. Sugita, M. Shoya, Adsorption of lead and mercury by rice husk ash, J. Colloid Interf. Sci. 278 (2004) 1–8.
[11] IS 1350 part I, 1984. Methods of Test for Coal and Coke, Proximate Analysis. Bureau of Indian Standards, Manak Bhawan, New Delhi, India.
[12] S. Brunauer, P.H. Emmet, F. Teller, J. Am. Chem. Soc. 60 (1938) 309.
[13] E.P. Barret, L.G. Joyer, P.P. Halenda, The determination of pore volume and area distributions in porous substances: 1. Computations from nitrogen isotherms, J. Am. Chem. Soc. 73 (1951) 373–380.
[14] L.S. Balistrieri, J.W. Murray, The surface chemistry of goethite (α-FeOOH) in major ion seawater, Am. J. Sci. 281 (6) (1981) 788–806.
[15] IUPAC Manual of Symbols and Terminology of Colloid Surface, Butterworths, London, 1982. p. 1.
[16] M.M. Abou-Mesalam, Sorption kinetics of copper, zinc, cadmium and nickel ions on synthesized silico-antimonate ion exchanger, Colloids Surf. A: Physicochem. Eng. Aspects 225 (2003) 85–94.
[17] M.M. Davila-Jimenez, M.P. Elizalde-Gonzalez, A.A. Pelaez-Cid, Adsorption interaction between natural adsorbents and textile dyes in aqueous solution, Colloids Surf. A: Physicochem. Eng. Aspects 254 (2005) 107–114.
[18] S. Ricordel, S. Taha, I. Cisse, G. Dorange, Heavy metals removal by adsorption onto peanut husks carbon: characterization, kinetic study and modeling, Sep. Purif. Technol. 24 (2001) 389–401.
[19] Y.S. Ho, C.C. Chiang, Y.C. Hsu, Sorption kinetics for dye removal from aqueous solution using activated clay, Sep. Sci. Technol. 36 (11) (2001) 2473–2488.
[20] H.A. Elliott, C.P. Huang, Adsorption characteristics of some Cu(II) complexes on alumino silicates, Water Res. 15 (1981) 849–854.
[21] D.L. Dugger, J.H. Stanton, B.N. Irby, B.L. McDonnell, W.W. Cummings, R.W. Maatman, Exchange of twenty metal ions with weakly acidic silanol group of silica gel, J. Phys. Chem. 68 (1964) 757–760.
[22] S.M. Lee, P.D. Allen, Removal of Cu(II) and Cd(II) from aqueous solution by seafood processing waste sludge, Water Res. 35 (2001) 534–540.
[23] N. Khalid, S. Ahmad, S.N. Kiani, J. Ahmed, Removal of lead from aqueous solutions using rice husks, Sep. Sci. Technol. 33 (1998) 2349–2362.
[24] Y.S. Ho, G. McKay, Pseudo-second order model for sorption processes, Process Biochem. 34 (1999) 451–465.
[25] T. Mathialagan, T. Viraraghavan, Adsorption of cadmium from aqueous solutions by perlite, J. Hazard. Mater. B94 (2002) 291–303.
[26] V.C. Taty-Costodes, H. Fauduet, C. Porte, A. Delacroix, Removal of Cd(II) and Pb(II) ions from aqueous solutions, by adsorption onto sawdust of *Pinus sylvestris*, J. Hazard. Mater. B105 (2003) 121–142.
[27] V. Padmavathy, P. Vasudevan, S.C. Dhingra, Biosorption of nickel(II) ions on Baker's yeast, Process Biochem. 38 (2003) 1389–1395.
[28] W.J. Weber Jr., J.C. Morris, Kinetics of adsorption on carbon from solution, J. Sanitary Engg. Div. ASCE 89 (SA2) (1963) 31–59.
[29] K. Kannan, M.M. Sundaram, Kinetics and mechanism of removal of methylene blue by adsorption on various carbons—a comparative study, Dyes Pigments 51 (2001) 25–40.
[30] J. Crank, The mathematics of diffusion, 84, first ed., Oxford Clarendon Press, London, 1965.
[31] G. McKay, M.S. Otterburn, A.G. Sweeney, The removal of colour from effluent using various adsorbents—III Silica: Rate processes, Water Res. 14 (1980) 15–20.
[32] G.E. Boyd, A.W. Adamson, L.S. Meyers, The exchange adsorption of ions from aqueous solution by organic zeolites. II Kinetics, J. Am. Chem. Soc. 69 (1947) 2836–2848.
[33] A.H.P. Skelland, Diffusional Mass Transfer, Wiley, NY, 1974.
[34] T. Vermeulen, Theory for irreversible and constant pattern solid diffusion, Ind. Eng. Chem. 45 (8) (1953) 1664–1670.
[35] J.-P. Chen, W.-R. Chen, R.-C. Hsu, Biosorption of copper from aqueous solutions by plant root tissues, J. Ferment. Bioeng. 81 (5) (1996) 458–463.
[36] J.P. Chen, M. Lin, Equilibrium and kinetics of metal ion adsorption onto a commercial H-type granular activated carbon: experimental and modeling studies, Water Res. 35 (10) (2001) 2385–2394.
[37] B. Chen, C.W. Hui, G. Mckay, Film-pore diffusion modeling for the sorption of metal ions from aqueous effluents onto peat, Water Res. 35 (14) (2001) 3345–3356.
[38] K.K.H. Choy, D.C.K. Ko, C.W. Cheung, J.F. Porter, G. McKay, Film and intraparticle mass transfer during the adsorption of metal ions onto bone char, J. Colloid Interf. Sci. 271 (2004) 284–295.